Science of the Total Environment 689 (2019) 457–468

Contents lists available at ScienceDirect

Science of the Total Environment

journal homepage: www.elsevier.com/locate/scitotenv

Optimized synthesis of a core-shell structure activated carbon and its adsorption performance for Bisphenol A

Pamphile Ndagijimana [a,b], Xuejiao Liu [a,b], Zhiwei Li [a], Guangwei Yu [a,*], Yin Wang [a,*]

[a] CAS Key Laboratory of Urban Pollutant Conversion, Institute of Urban Environment, Chinese Academy of Sciences, Xiamen 361021, China
[b] University of Chinese Academy of Sciences, Beijing 100049, China

HIGHLIGHTS

- The core-shell structure activated carbon was successfully optimized.
- CSAC applied on adsorbing of BPA from aqueous solutions.
- The Shell generated from small particles size of KL-400 showed a better protection of AC core.
- The adsorption of BPA on CSAC depends on both physical and chemical interactions.

GRAPHICAL ABSTRACT

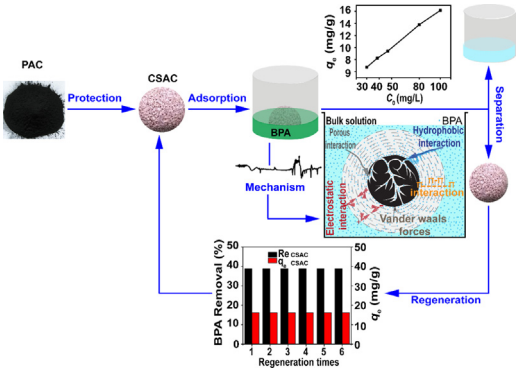

ARTICLE INFO

Article history:
Received 29 April 2019
Received in revised form 14 June 2019
Accepted 15 June 2019
Available online 19 June 2019

Editor: Huu Hao Ngo

Keywords:
Activated carbon
Adsorption
Bisphenol A
Core-shell structure
Porous ceramic shell

ABSTRACT

The presence of endocrine disrupting chemicals (EDCs) in the environmental water poses a serious threat which requires strong practical solutions. The existing activated carbon-based adsorbents exhibit a number of limitations hindering for their use in adsorption in an aquatic environment. In this work, a controlled technique was used to make a protected Core-Shell structure Activated Carbon (CSAC) material with a smaller size (0.82 cm), thinner shell thickness (0.083 cm) and high mechanical strength (2.41 MPa). The experimental results demonstrated that the sizes of shell precursors used for preparing the ceramic shell had a pronounced influence on the produced material. The shell was prepared by using a mixture of kaolinite (400 mesh) and coal fly ash (100 mesh). The pellet activated carbon core was synthesized by a pelletizing method using powder activated carbon (92%) mixed with the binder (8%) from cassava splinters. The kinetic study evidenced that the performance of the material fitted better for pseudo-second-order kinetic and the intraparticle diffusion. Furthermore, the maximum amount of Bisphenol A (BPA) adsorption by CSAC fitting to Langmuir model was 28.5 mg g^{-1}. The BPA adsorption by CSAC was an endothermic process. Therefore, this material could be applied in the remediation of various aquatic EDCs.

1. Introduction

The presence and accumulation of endocrine disrupting chemicals (EDCs) in the aquatic environment are increasing. These substances

* Corresponding authors.
E-mail addresses: gwyu@iue.ac.cn (G. Yu), yinwang@iue.ac.cn (Y. Wang).

https://doi.org/10.1016/j.scitotenv.2019.06.235
0048-9697/

are known to cause severe risks to living things because of their abilities to interfere with biological activity by binding on hormone receptors, transport, and metabolic processes of natural hormones (Chen et al., 2013; Lagana et al., 2004; Xu et al., 2012). Bisphenol A (BPA) is one of the EDC groups applied in manufacturing of various polymers and plastic products (Kang et al., 2006). The presence of BPA in the ecosystem are derived from inadequate or non-treatment of industrial waste and municipal effluent (Arnold et al., 2013; Corrales et al., 2015). It is still evidenced in the surface water, (Jin and Zhu, 2016), groundwater (Careghini et al., 2015; Li et al., 2015), drinking water (Staples et al., 2000), and soil (Inoue et al., 2008). This is due to its non-biodegradability nature and makes it a persistent antioxidant in the environment. Previous findings reported that the low dose of BPA in humans caused prostate cancer cell, heart diseases, diabetes and abnormalities in liver enzymes (Hugo et al., 2008) as well as a threat to aquatic organisms (Soares et al., 2008). Therefore, it is greatly required to develop a sustainable and green technology to eliminate BPA in the aquatic environment.

Various technologies for BPA treatment were introduced, such as ultrafiltration, coagulation, reverse osmosis, chemical, biological methods, photoelectrocatalytic, adsorption (Brugnera et al., 2010; Chen et al., 2006; Heo et al., 2012; Liu et al., 2009; Toledo et al., 2005). Among these technologies, adsorption technique was proven to be an effective method to eliminate the BPA in water and have several advantages over the mentioned techniques, including affordable operations and environmental-friendly (López-Ramón et al., 2019; Putra et al., 2009). Activated carbon (AC) is a well-known adsorbent and is commonly used in the form of a powder or granular (Delgado et al., 2012; Kavitha and Namasivayam, 2007). The powder activated carbon (PAC) is generally considered as the most efficient material to control organic contaminants in water due to its large specific surface area and hydrophobic surface (Choi et al., 2005; Nakanishi et al., 2002; Tsai et al., 2006). However, the small particle size of PAC turned into a colloidal solution as residual PAC which limits its application and effective recovery from the treated water system (Choi et al., 2005; Wu et al., 2015). Moreover, PAC residuals are considered as a secondary pollutant in the aquatic system which can lead to a high-pressure drop in the filtration system (Çeçen and Aktas, 2011). Therefore, new techniques are required to conquer these limitations. Briefly, the main obstacles are insufficient ability to recover and regenerate PAC from the aqueous medium. Currently, several studies on the recovery and regeneration of PAC reported that the regeneration of PAC led to the decreasing overtime of adsorption performance and the degeneration of the material (Gong et al., 2016; Salvador et al., 2015a; Salvador et al., 2015b; Marques et al., 2017; Yuan et al., 2016).

A promising way of guaranteeing long-term usage and avoiding possible degeneration of PAC is to protect it by a core-shell structure with good compressive strength. In our previous work, a novel shell was synthesized using coal fly ash and clay and it exhibited a good protection function to the AC core (Ndagijimana et al., 2019). However, we also found that the size of the porous channel of the shell was still large enough to release out some fraction of the AC core during the liquid adsorption. Additionally, the application of the prepared core-shell structure material was limited by its heavyweight (thick shell) and big size. A qualified core-shell activated carbon (CSAC) material should simultaneously possess high compressive strength and a good protection of AC core, as well as thinner shell thickness. The thinner shell thickness has a shorter pathway for the mass diffusion and transport to the inner surface. Based on aforementioned problems, the following work were conducted in this study: (i) to optimize the synthesis of CSAC by controlling its raw materials' particle size of the shell (kaolinite; KL and coal fly ash; CFA) resulting into a shell with appropriate size of porous channel, high compressive strength and thinner shell thickness; (ii) to evaluate the performance of the optimized material through adsorbing BPA and studying its efficiency in co-adsorption of multiple organic contaminants (antibiotics, BPA) in aqueous solution; and (iii) to illustrate BPA adsorption mechanisms by studying the kinetics, isotherms and surface composition of the material.

2. Experimental section

2.1. Materials

The details of materials and chemicals used in this work (kaolinite, coal fly ash, powder activated carbon, Cassava Waste splinters (CWS) for cassava splinters binders (CSB) preparation and Bisphenol A) are shown in (Ndagijimana et al., 2019). The preparation of CSB was described in supporting information Text S1. The chemical compositions of KL and CFA were listed in Table S1, while the chemical elements for CSB, CWS, PAC and AC core are shown in (Ndagijimana et al., 2019). Furthermore, the properties of BPA were illustrated in Table S2.

2.2. Preparation method of CSAC

The procedures for AC core1 and core-shell AC pellet preparation were presented in details in our previous study (Ndagijimana et al., 2019). Furthermore, the summary of this procedure was presented in supporting information Text S2.

To optimize the aforementioned properties (particle size, thickness, and compressive strength), the CSACs pellets with different particles size mixture of KL-CFA on the shell were prepared as follows: firstly, the particle size of KL and CFA were sieved into different meshes such as 100, 200 and 400-meshes and 100, 200 and 325-meshes, respectively. Thereafter, the different particle size of KL and CFA were mixed (KL-CFA) by ratio of 60%:40% as follows: 200-mesh for KL without CFA, 200–325, 200–200, 200–100, 100–100 and 400–100-meshes (namely KL-100 to KL-400 and CFA-100 to CFA-325) then after the CSACs pellets were dried, preheated and sintered according to the procedures in previous study.

2.3. Characterization

The characterization of samples was explained in supporting information Text S3.

2.4. Adsorption of BPA

Batch adsorption analysis was performed by 0.24 g of CSAC as adsorbent added in 100 mL of the adsorbate solution, contained in a conical flask in water bath oscillation, at an agitation rate of 180 $r \cdot min^{-1}$, an initial pH of 7.0 for 24 h and at 25 °C. The remaining solution of BPA after adsorption was filtrated via a 0.45 μm pore size membrane of cellulose membrane. The filtrate was proved with high-performance liquid chromatography (HPLC) at 25 °C and a wavelength of 225 nm, with the help of an Extend-C18 column (250 mm × 4.6 mm, 5-Micron 80 A) from Agilent (USA). The mobile phase was 50% pure water and 50% acetonitrile mixed with 2 mL of acetic acid with a volume proportion of 50:50, at a flow rate of 0.6 mL min^{-1} through the column. The retention time of BPA was 5–6 min (with a run time of 7 min). To analyze the effect of the contact time, samples of BPA solution with a concentration of 100 mg/ L were withdrawn at a specific time during the 600 min periods at pH = 7 and 25 °C. The effects of different initial concentrations of BPA solution at 30, 40, 50, 80 and 100 mg/ L were tested at an initial pH of 7.0 and at 25 °C. The different pH solution values at 1.0, 2.0, 4.0, 5.6, 7.0, 9.0 and 12.0 were prepared by regulating the initial solution by caustic soda (NaOH) or hydrogen chloride (HCl). The effect of these pH ranges was analyzed at an initial concentration of 100 mg/L at 25 °C. The influence of ionic strength on BPA adsorption was executed in NaCl solutions at 0.01, 0.05, 0.10 and 0.50 mol L^{-1}. The effects of temperature were also investigated at different temperature of 25, 45 and 65 °C. To ensure the reusability of adsorbents, the spent CSAC were regenerated. Then, the regenerated adsorbent was reused for another adsorption attempt.

The comparison of the BPA removal efficiency with that of the different antibiotics (sulfamethoxazole, tetracycline, and oxytetracycline) by CSAC were tested in 100 mg/L of the solution. In addition, the competition effect was studied in 10 mg/L of a solution containing the aforementioned adsorbates to evaluate the performance of the optimized material in co-adsorption of multiple organic contaminants in aqueous solution. The kinetics and isotherm models were applied to fit the adsorption data of BPA by a protected activated carbon (CSAC) (Mittal et al., 2010; Peng et al., 2015; Wang et al., 2018; Wirasnita et al., 2014). Furthermore, the thermodynamic study was further investigated (Arampatzidou and Deliyanni, 2016). The kinetic and isotherm models were discussed in supporting information Text S4.

3. Results and discussion

3.1. Optimization and characterization of CSAC

In this research, the effect of particles size of KL and CFA on CSAC was evaluated to control the size, the shell thickness, mechanical strength, as well as protection of the AC core. The physical images of CSACs obtained after sintering at 1250 °C were presented in Fig. 1. It showed that the textural property of the fabricated shell depends on the particles size of KL and CFA. Fig. 1a showed the CSAC had no porous structure on the shell by naked eyes caused by the absence of CFA which was a pore forming agent. The CSACs with dark-gray color were produced using the K-CFA mixture sieved at 200–325, 200–200, 200–100 (Fig. 1b–d), black color at 100–100 meshes (Fig. 1e) and dark chestnut (Fig. 1f) using 400–100 meshes after sintering at 1250 °C. The materials obtained using CFA (Fig. 1b–f) all presented the porous structures on the shell, indicating CFA was the pore-forming agent. Fig. 2a depicted that the CSAC obtained from KL-400 (smallest size) has a thinner thickness (0.083 cm). This indicated that a thinner shell could be produced with a smaller particle size of KL. This phenomenon was possibly due to the presence of small intra-particle space and strong contact point in the ceramic shell after sintering at 1250 °C. The shell generated by small particles size of KL-400 exhibited a high compressive strength of 2.41 MPa (Fig. 2b). This phenomenon demonstrated that the sizes of the shell precursors affected the mechanical strength of the core-shell AC. This was derived from the existence of stronger contact points or cohesion in the porous ceramic shell to construct a compact shell structure. Moreover, the same observation could be supported by SEM imaging (Text S5; Fig. S1) which showed that the shell synthesized using a bigger particles size of KL-CFA (100–100 meshes) resulted into an increased voids size (Fig. S1e). As for the water absorption test (Figs. 2 and S2), it was observed that the increased bubbles in the solution evidenced the absorption of water through the porous ceramic shell and this absorption was much pronounced for the thinner shell (Fig. S2e) obtained by a composition mixture of KL-400 and CFA-100. It was pointed out by Bicer (Bicer, 2018) that as the grain size diameter of fly ash decreased, ash density increased as well, the porous structure could be replaced by full-grain ash (pore blockage) which affected water absorption efficiency. Finally, we applied the synthesized CSACs materials in the adsorption of BPA as shown in Fig. 2d. It can be seen that the adsorption capacity increased with the particles size of KL-

Fig. 1. Effect of KL-CFA particles size on CSAC after sintering at 1250 °C.

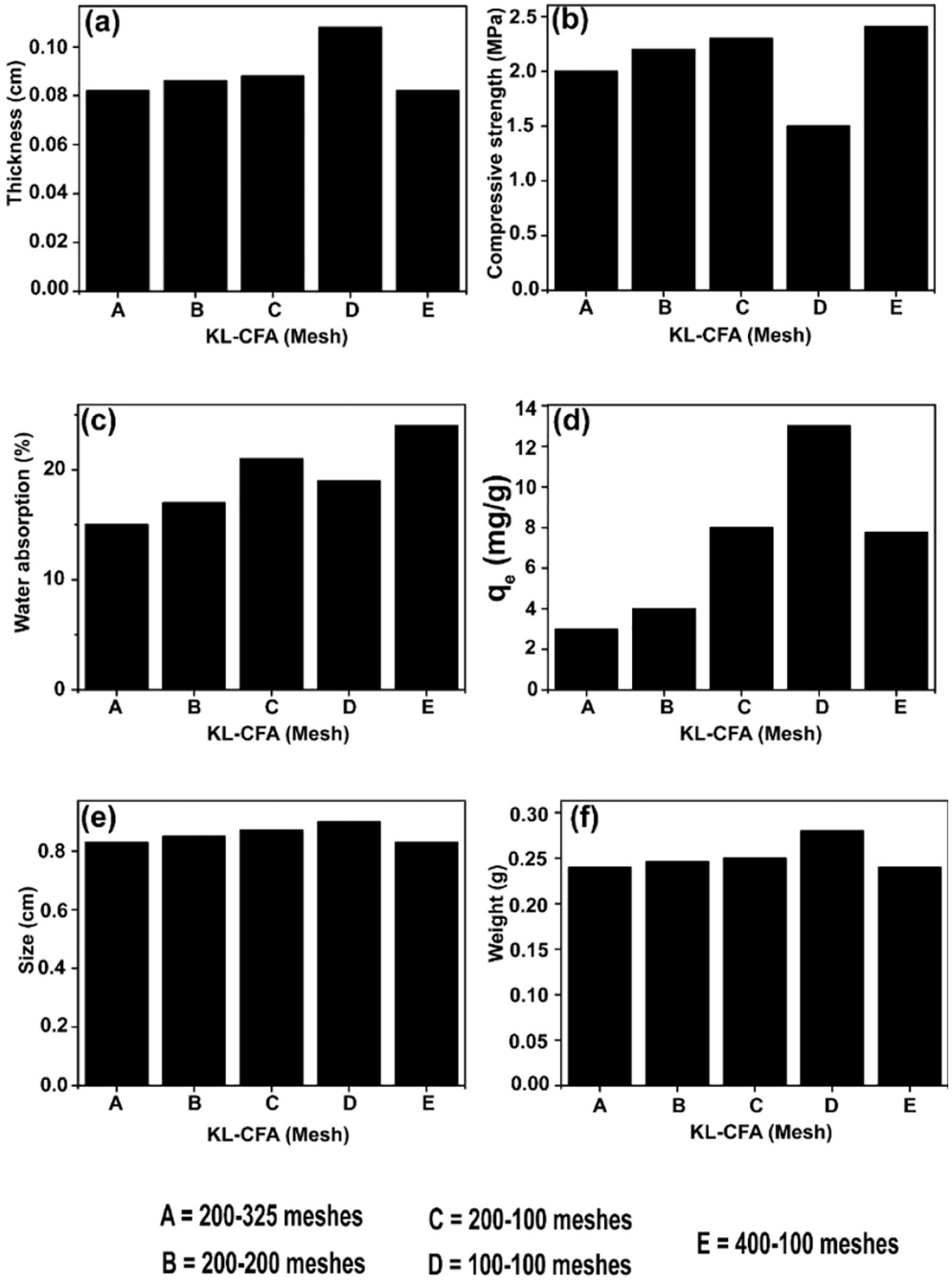

Fig. 2. Effect of particles size on shell thickness (a), compressive strength (b), water absorption (c), BPA adsorption (d), size (e), and weight of CSAC (f).

CFA. Though the adsorption capacity of BPA increased, it was observed that some fraction of the AC core was easily released out into the solution at high shaking rate (180 rpm), affecting its performance and reusability overtimes. This was related to the wide voids and intra-particle space in the shell which confined much less mechanical protection of the core. However, as for the optimized material, this phenomenon was not observed because of the small intra-particles space, hence the protection of the core from outflow during the adsorption process. Furthermore, the size and weight of the samples were evaluated as shown in Fig. 2e and f. The KL-400 material presented smaller size and lightweight, and this was due to using small particle size of KL. Therefore, the corresponding sample with a small particle size of KL-400 was determined as the optimized sample.

For further characterization of the optimized sample (namely the sample obtained from KL-400 and CFA-100), the sample morphology was examined by SEM (Fig. 3). As shown in Fig. 3a–b the pores and intra-particle void/space were observed on the ceramic shell. The images of the CSAC could be visually seen in Fig. 3c. The capillary-like pore structures were found on the surface of AC core (Fig. 3d). The crystalline states of KL, CFA and porous ceramic shell were analyzed by X-ray diffractograms (Fig. 4). Fig. 4a showed the presence of dolomite, quartz, and diaspore in the raw material of CFA and kaolinite mineral was found in KL. Fig. 4b showed the XRD patterns of the CSAC (shell), the result indicated the presence of anorthite, mullite, and hawaite. Furthermore, the mechanical strength of CSAC was tested as 2.41 MPa (Fig. 2b). The good mechanical strength was likely due to the stronger contact points in porous ceramic shell derived from the small particle size of KL and the formation of the quartz phase, crystallization towards the formation of new mineral such as mullite and glass phases at 1250 °C. The zeta potential of the adsorbent surface was analyzed and calculated to be $pH_{pzc} = 1.88$

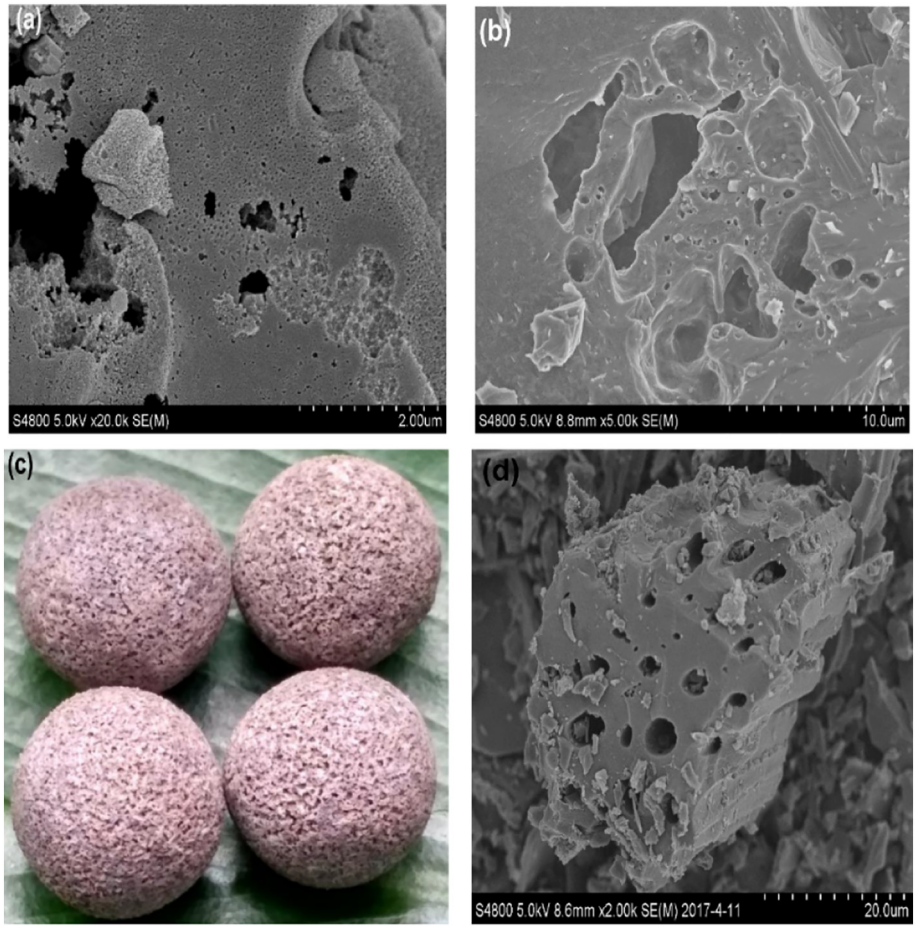

Fig. 3. SEM images of the ceramic shell's surface (a), intra-particle space or voids (b), images of CSAC (c), and AC core2 (d).

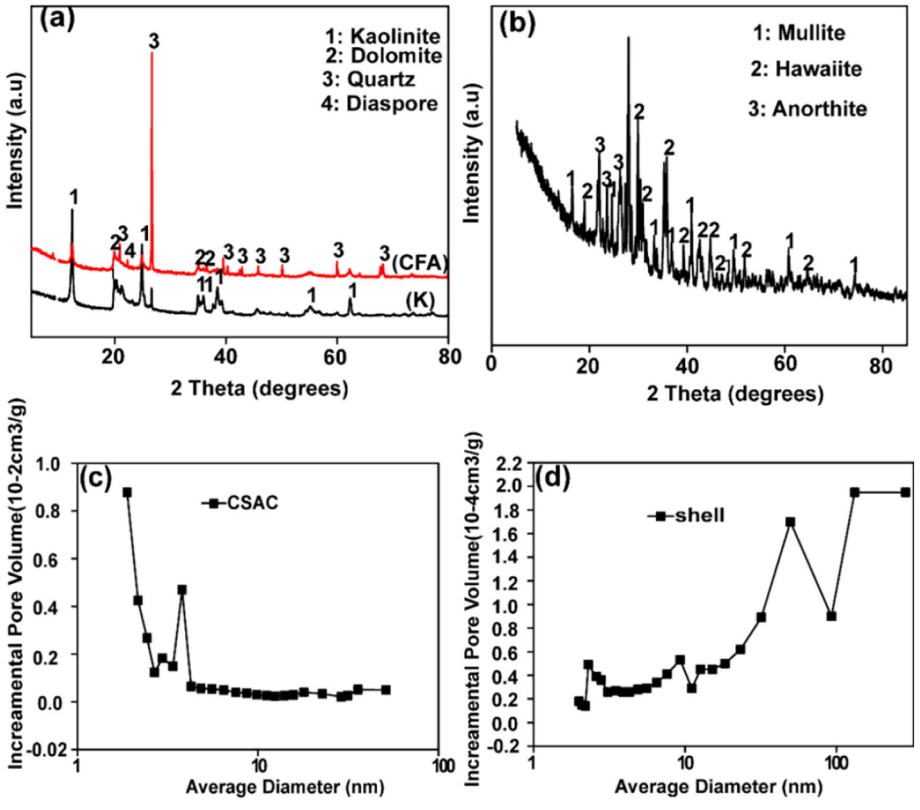

Fig. 4. X-ray diffraction patterns for coal fly ash and kaolinite (a), ceramic shell (b), pore distribution for CSAC (c), and shell after sintering at 1250 °C (d).

Table 1
Surface area (S_{BET}), pore volume and pore size of the core-shell activated carbon.

Sample	S_{BET} ($m^2\ g^{-1}$)	Pore volume ($cm^3\ g^{-1}$)	Pore size (nm)
CSAC[a]	199.00	0.11	2.25
Shell	0.99	11×10^{-3}	4.59
KL-CFA[b]	19.42	0.11	21.00

[a] Core-shell activated carbon.
[b] Mixture of kaolinite and coal fly ash.

(Ndagijimana et al., 2019). The specific surface area (S_{BET}), pore size and pore volume for CSAC, shell and KL-CFA were listed in Table 1, and for the AC core (referred to as AC core 2 in our previous study) and PAC were presented in our previous study (Ndagijimana et al., 2019). The S_{BET} of the CSAC was 199 $m^2\ g^{-1}$. The S_{BET} decrease of CSAC vis-à-vis AC core2 without the shell was caused by the protection by the shell (Ndagijimana et al., 2019). The calculated S_{BET} of the separated shell was 0.985 $m^2\ g^{-1}$, while the S_{BET} of shell precursors (KL-CFA) before sintering at high temperature was 19.42 $m^2\ g^{-1}$. The pore volume and pore size of the precursor mixture of the shell reduced after the material was sintered at 1250 °C (Table 1). Fig. 4c–d presented the pore size distributions and average pore size. The pore size distribution displayed the micro-mesopore and macropore (Fig. 4c). Fig. 4d showed the pore distribution of the shell detached from CSAC after sintering at 1250 °C. This result indicated that the shell displayed a broad pore size distribution, however the macropores distribution increasing after sintering at 1250 °C.

3.2. Application for BPA removal from aqueous solution

3.2.1. Effect of initial BPA concentration

Fig. 5a illustrated the effects of the initial concentration of BPA solution and showed the corresponding BPA removal efficiency by CSAC was 54.0, 49.0, 45.0, 41.4, and 38.8%, respectively. On the other hand, the percentage of BPA removal by AC core was 100, 99.70, 95.78, 82.00 and 74.76%, respectively. Furthermore, for PAC, the BPA removal efficiency was 100, 99.35, 94.18, 80.29, and 74.32%, respectively. The adsorption capacity (q_e) for CSAC were 6.74, 8.24, 9.39, 13.79 and 16.16 mg g^{-1}; while for it was 59.60, 79.78, 95.78, 130.52 and 149.52 mg g^{-1} AC core, and 59.13, 79.48, 94.18, 128.46 and 148.64 mg g^{-1} for PAC, respectively. The percentage of BPA removal decreases as its initial concentration increases. This is ascribed to the constant adsorptive sites on the adsorbent which is insufficient after increasing the adsorbate initial concentration. This phenomenon observed in many other studies (Tan et al., 2008; Tsai et al., 2006; Wirasnita et al., 2014). The removal percentage (%R) and adsorption capacity (q_e) of BPA on AC core separated from CSAC were better than for PAC. This is led to the increasing of S_{BET} for AC core after sintering at high temperature. Furthermore, the protected activated carbon (CSAC) keeps exhibiting potential feasible separation and reusability.

3.2.2. Effect of ionic strength on adsorption of BPA

The effect of ionic strength on BPA adsorption is presented in Fig. 6a. It is illustrated that the adsorption capacity increased using NaCl at 0.1 mol L^{-1}. Then it decreased slightly from 0.1 to 0.5 mol L^{-1}. Results demonstrated that the BPA adsorption was slightly affected by the ionic strength. Ionic effect phenomena is explained as follow: Firstly, the electrostatic screening effect of the surface charge generated from the increasing of ionic strength will favor adsorbate-adsorbent dispersion interactions, then enhance the adsorption of BPA. Secondly, the raising of ionic strength promotes the salting-out effect which leads to the low solubility of BPA as well as promoting its hydrophobicity, thus, increasing its sorption by the adsorbent. Thirdly, the increase of the ionic concentration may lead to the occupation of active sites (squeezing-out effect) of adsorbents and hinder the adsorption of BPA. As such, the adsorption amount was reduced when the concentration of NaCl was higher than 0.1 M. It shows that NaCl also competed with BPA on the adsorption sites of the CSAC and other adsorbents, and the active sites for BPA were then filled by NaCl. This correlates with what was reported (Wang et al., 2017).

3.2.3. Effect of initial pH

The solution pH is a critical factor for the adsorption process in the aqueous phase because it determines the surface charge of adsorbate-adsorbent. Fig. 6b depicts the effect of pH on the adsorption of BPA by CSAC, AC core, and PAC. According to the zeta potential of the CSAC

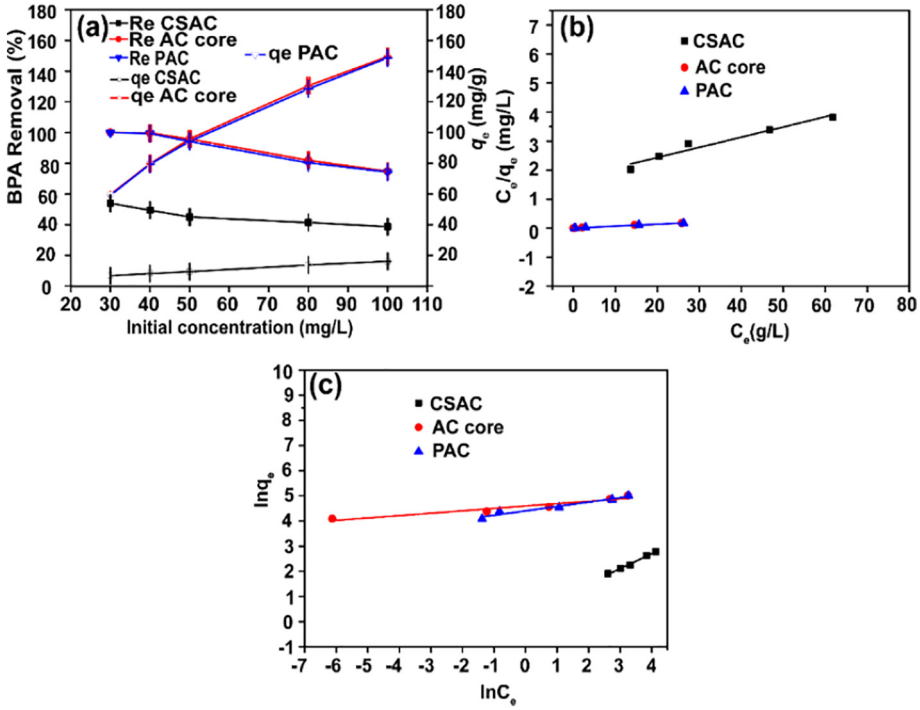

Fig. 5. Effect of initial concentration (a), Langmuir (b), and Freundlich fitting model (c).

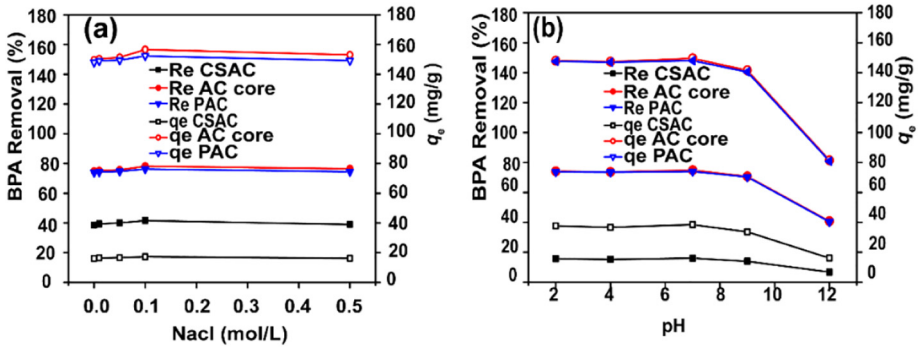

Fig. 6. Effect of ionic concentration (a) and pH (b).

($pH_{pzc} = 1.88$), the surface charge of the CSAC, AC core, and PAC became negative when the solution pH value was more than pH_{PZC}. On the contrary, the surface charge was positively charged when the solution pH value was less than the pH_{PZC}. At pH lower than 9 most of BPA did not dissociate and existed in molecular form, while BPA was deprotonated to bisphenolate anion at very basic pH. Thus, the pH of the solution generally did not affect the removal of BPA from a pH range of 2 to 7. However, from a pH range of 9 to 12, the amount of BPA adsorption diminished. The reduction in the adsorption amount of BPA on the CSAC, AC core, and PAC examined at high pH values is resulted to the repulsive electrostatic interacting within the anionic adsorbent surface and the anion BPA (BPA^-). This phenomenon correlates with findings reported by studies (Wang et al., 2018; Wirasnita et al., 2014).

3.2.4. Effect of contact time

As depicted in Fig. 7a, the amount of adsorption promoted with contact time and reaches the equilibrium between 540 and 600 min for CSAC. It was explained that the solution firstly cross ceramic shell to the AC core and then got into the AC core until it attained the equilibrium. The adsorption process for AC core detached from shell showed that its removal rate was initially quick (~120 min) and then reduced until to attain equilibrium time of around 240 min. The rapid adsorption within the first 120 min was associated with the readily accessible sites. Finally, equilibrium was reached after 240 min, hence the proof of the saturation of the AC core. Indeed, the adsorption of BPA by PAC shows that the rate was initially quick and then decreased until to attain an equilibrium time of around 60 min, which was faster than both of situations of a protected adsorbent and AC core. This was because of the large exposure active sites on PAC and the fast BPA mass diffusion through the PAC.

3.3. Adsorption kinetics and isotherm

3.3.1. Adsorption kinetics

The kinetic model was applied to study the rate of BPA adsorption by CSAC. Table 2 shows the kinetics parameter data. By plotting $\ln(q_e - q_t)$ vs t and t/q_t vs t (Fig. 7b), the correlation coefficients (R^2), kinetics constant (k_1) and q_e values can be calculated. The pseudo-second-order

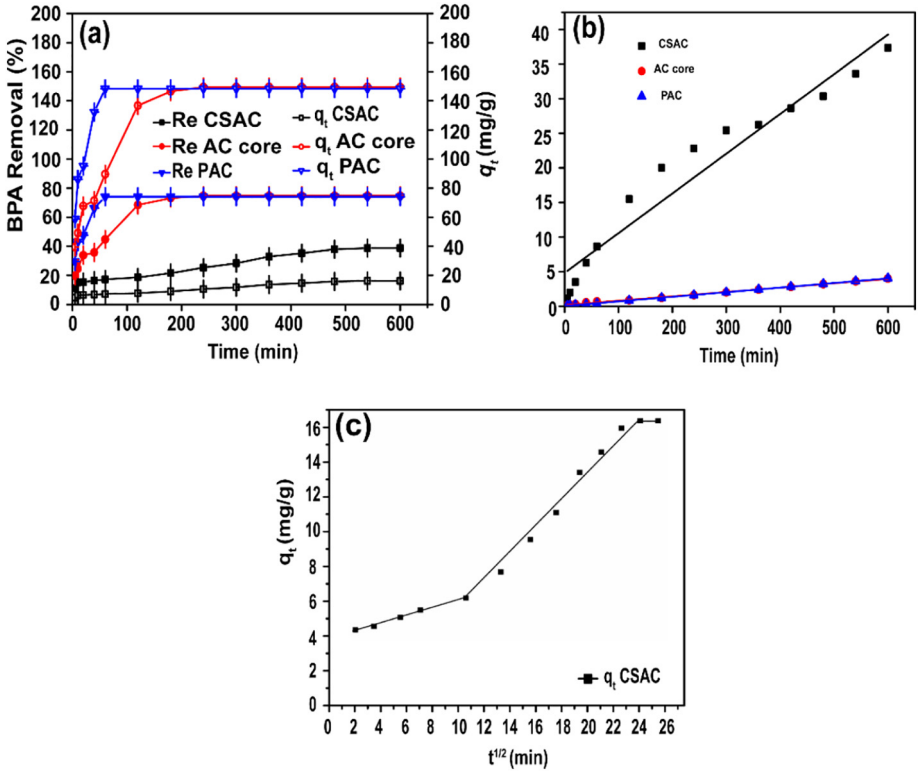

Fig. 7. Effect of contact time (a), curves of fitting pseudo-second-order adsorption kinetics (b), and intra-particle diffusion (c).

Table 2
The kinetic parameters of bisphenol A adsorption.

Kinetic model	Parameters		
	CSAC	AC-core	PAC
q_e experimental (mg g^{-1})	16.10	149.50	148.30
Pseudo-first-order			
q_e calculated (mg g^{-1})	14.00	132.00	96.70
K_1	0.006	0.018	0.010
R^2	0.800	0.928	0.677
Pseudo-second-order			
q_e calculated (mg g^{-1})	17.00	158.00	151.50
K_2	0.015	47×10^{-6}	15×10^{-5}
R^2	0.936	0.997	0.999
Intraparticle-diffusion			
C	5.684	86.00	93.60
K_{dif}	0.019	0.185	2.900
R^2	0.972	0.619	0.530

kinetic model presented better fitting according to the small difference between (q_e^{exp}) and (q_e^{cal}) (Table 2). This result is in agreement with several literatures on adsorption of organic solutes by activated carbons (Ghaedi et al., 2013; Tonucci et al., 2015). Diffusion mechanism was explained by the intraparticle diffusion model (Supporting Information Text S4). According to the high correlation coefficients ($R^2 = 0.972$) values shown in Table 2, the adsorption process was also probably controlled by the intraparticle diffusion. The plot of q_t versus $t^{1/2}$ (Fig. 7c) was multi-linear suggesting the presence of three steps in the adsorption process. These findings agree with the report presented by (Wang et al., 2018). Fast external surface adsorption, gradual inner-core surface adsorption and final equilibrium are key steps for the adsorption of organic adsorbate by CSAC and are explained in details in our previous work (Ndagijimana et al., 2019).

3.3.2. Adsorption isotherm

The adsorption isotherm model was used to study the interaction between adsorbate and adsorbents at a certain temperature. The data for Langmuir and Freundlich were explained and presented in Table 3. The values of q_m and k_L were determined from the slope and intercept of a linear plot of c_e/q_e versus c_e (Fig. 5b), where the slope is equal to $1/q_m$ and intercept is equal to $1/q_m k_L$. The slope and intercept obtained from the plot of $\ln q_e$ against $\ln C_e$ (Fig. 5c) yield the Freundlich constants (k_F and n). According to their average correlation coefficients (R^2), the Freundlich isotherm depicted the adsorption data better than the Langmuir isotherm model. Langmuir isotherm model fits better to AC core and PAC, which is the proof of the monolayer adsorption process. Then, values in Table 3 indicated moderate adsorption of BPA by CSAC and good adsorption for AC core and PAC. The maximum adsorption amount of adsorbents for adsorbate was estimated by the Langmuir model (Table 3).

For the comparison with the adsorption capacities of other adsorbent material (Table 4), the adsorbents in this work have a relatively good adsorption capacity.

Table 3
The adsorption isotherm parameters of bisphenol A adsorption.

Adsorption isotherm model	Parameters		
	CSAC	AC core	PAC
Langmuir isotherm			
q_m (mg g^{-1})	28.50	148.60	149.00
k_L (L/ mg)	1.70	3×10^{-5}	5×10^{-4}
R^2	0.940	0.991	0.989
Freundlich isotherm			
k_F (mg g^{-1}) $(L/mg)^{1/n}$	1.39	98.95	81.50
N	1.70	10.00	6.00
R^2	0.990	0.903	0.942

Table 4
Comparison of bisphenol A adsorption capacity onto several adsorbents.

Sample	Adsorption capacity q_m (mg g^{-1})	Reference
PAC	149.00	This work
AC core 2	148.60	This work
CSAC	28.50	This work
Modified fibric peat	29.20	(Zhou et al., 2011)
Andesite	0.50	(Tsai et al., 2006)
Diatomaceous earth	0.70	(Tsai et al., 2006)
Graphene	182.00	(Xu et al., 2012)
Sugi chip	11.50	(Nakanishi et al., 2002)
Sugisawadust	12.10	(Nakanishi et al., 2002)
Almond shell AC	188.90	(Nakanishi et al., 2002)

3.4. Influence of temperature and thermodynamic study

The influence of temperature on adsorption of BPA was investigated at a temperature of 25, 45 and 65 °C. The Fig. 8a shows the data parameters of the temperature effect, the observation showed that the amount of adsorbed BPA on CSAC and AC core favored as temperature increased, hence, the endothermic process is proven. This is owing to the enhancing of the diffusion rate for BPA solution throughout the external boundary layer and internal pores materials (CSAC and AC core). Moreover, it is related to the decreasing in the viscosity of the solution for highly concentrated suspensions at high temperature. This phenomenon correlates with the reported finding by the study (Dogan et al., 2009). The parameters of experimental data fitting to Langmuir and Freundlich isotherm are illustrated in Table 5. The q_m and the K_F were increased as the temperature was increased, revealing that higher temperature favors the BPA removal. On the contrary, the removal of BPA on PAC decreased as the temperature increased. This clarified the exothermic process, and the q_m and the K_F values were also reduced. This likely led to the lowering of the adsorptive forces between the binding sites on the PAC and the BPA adsorbate. This phenomenon correlates with the reported finding (Dogan et al., 2009; Javed et al., 2018; Ofomaja and Ho, 2007).

The thermodynamic parameters including the enthalpy change ΔH^o (KJ mol^{-1}), entropy ΔS^o (J mol^{-1} K) and the Gibbs free energy of adsorption ΔG^o (kJ mol^{-1}) were presented by Van't Hoff equations (Fan et al., 2013) (Eqs. (1) and (2)):

$$\ln\left(\frac{q_e}{C_e}\right) = -\frac{\Delta H^\circ}{RT} + \frac{\Delta S^\circ}{T} \quad (1)$$

$$\Delta G^\circ = -RT ln K_C \quad (2)$$

where T is the absolute temperature (in Kelvin) and R is the universal gas constant (8.314 J mol^{-1} K^{-1}). As presented in Fig. 8b the Plotting ln (q_e/c_e) versus 1/T showed a straight line with slope and intercept equal to $-\Delta H°/R$ and $\Delta S°/R$, respectively.

The positive value of $\Delta H°$ (Table 6) shows the endothermic nature of the adsorption process of BPA on AC core and CSAC while the negative value proving the exothermic adsorption process of BPA on PAC. The adsorption increased with the increasing the temperature and BPA is conductively adsorbed on the surface of CSAC. Gibb free energy of adsorption (ΔG°) is determined from the Eq. (2). The negative values of ($\Delta G°$) (Table 6) show that the adsorption reaction was spontaneous. The magnitude of ΔH^o may infer the type of adsorption. The heat developed during physical adsorption locates in the range of 2.1–20.9 kJ mol^{-1} and the range of 80–200 kJ mol^{-1} for chemisorptions (Chowdhury et al., 2011). The results are coherent with findings reported of previous reports (Berhane et al., 2016; Ofomaja and Ho, 2007).

3.5. Thermal regeneration study

This study was undertaken to ensure promising ways for the reuse of the material in the future. The CSAC after saturated was thermally

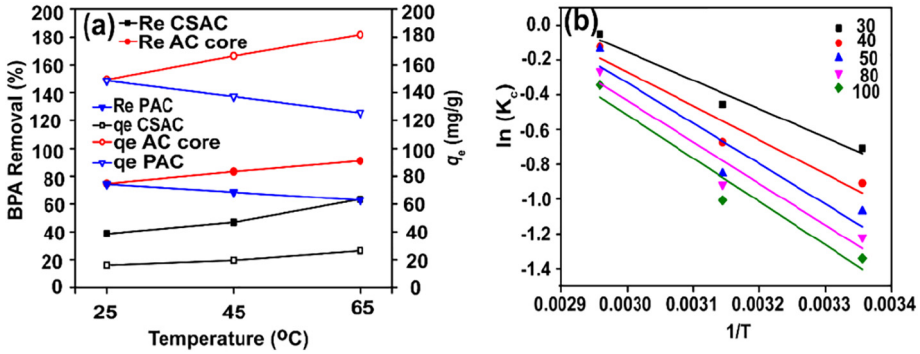

Fig. 8. Effect of temperature (a) and Plot of K_C versus 1/T for determination of BPA removal reaction enthalpy (b).

regenerated at 600 °C for 1 h to remove BPA contaminant. Regeneration cycle was repeated six cycles using the same process. As presented in Fig. 9, the reused adsorbent displayed a significant adsorption amount compared to the fresh adsorbent without losing the adsorption capability. Thus, the CSAC material is recommendable and promising adsorbent material for removing BPA from aqueous solutions.

3.6. Competition effect

Comparison of BPA removal by CSAC sample with other three kinds of antibiotics was investigated, including tetracycline, oxytetracycline, and sulfamethoxazole. Furthermore, the competition effect was also investigated. Fig. 10a showed that BPA presented higher removal efficiency in comparison to that of the other antibiotics. The removal percentage of single BPA, Sulfamethoxazole, tetracycline, and oxytetracycline by CSAC was 38.12, 31.00, 18.00, and 10.50%, respectively. Fig. 10b illustrated the competition effect. As shown in Fig. 10b, the removal percentage of the multi-component solution of 10 mg/L for BPA, sulfamethoxazole, tetracycline, and oxytetracycline was 30.76, 21.19, 12.23 and 7.78%, respectively. It demonstrated that the removal efficiency of adsorbate was decreased. This result indicated that the competition effect between these adsorbates existed.

Table 5
Effect of temperature on bisphenol A adsorption.

Isotherm Langmuir	Temperature (°C)	Constant		
		q_{max} (mg g^{-1})	K_L (L/ mg)	R^2
CSAC	25	28.5	1.74	0.940
	45	40	1.49	0.827
	65	81	0.89	0.810
Freundlich	Temperature (°C)	Constant		
		K_F (mg g^{-1}) (L/mg)$^{1/n}$	n	R^2
CSAC	25	1.39	1.70	0990
	45	1.42	1.50	0.975
	65	1.50	1.25	0.998
Isotherm Langmuir	Temperature (°C)	Constant		
		q_{max} (mg g^{-1})	K_L (L/ mg)	R^2
PAC	25	149	5×10^{-4}	0.990
	45	140.0	8×10^{-4}	0.959
	65	113.0	95×10^{-4}	0.917
Freundlich	Temperature (°C)	Constant		
		K_F (mg g^{-1}) (L/mg)$^{1/n}$	n	R^2
PAC	25	81.49	6	0.942
	45	66.80	5	0.838
	65	62.54	6	0.639
Isotherm Langmuir	Temperature (°C)	Constant		
		q_{max} (mg g^{-1})	K_L (L/ mg)	R^2
AC-core	25	148.60	3×10^{-4}	0.991
	45	167.78	18×10^{-4}	0.990
	65	185.50	11×10^{-4}	0.988
Freundlich	Temperature (°C)	Constant		
		K_F (mg g^{-1}) (L/mg)$^{1/n}$	n	R^2
AC-core	25	98.95	10	0.903
	45	110.00	9.8	0.875
	65	120.99	9.0	0.812

3.7. Possible mechanisms of BPA adsorption

The adsorption mechanism requires various interactions and is a complex process (Dogan et al., 2009; Wirasnita et al., 2014). Nevertheless, it still needs to be clarified following the results of the pore texture and chemical characteristics of the adsorbent, the nature of the solution and the hydrophobic nature of BPA (Toledo et al., 2005). Further, Wang et al. showed that the adsorption of BPA on AC may be studied by the π–π interaction, hydrogen bonding, and hydrophobic interaction (Wang et al., 2017). As illustrated in the conceptual figure (Fig. 11), possible mechanisms of BPA adsorption by CSAC can be explained as follows. Firstly, the BPA molecules pass through the porous channel of the shell which is confirmed by SEM image and BET analysis as well as the absorption of aqueous solution through the porous cermic shell as confimed by bubbles in Fig. S2. The transport of BPA molecules from bulk solution to the porous of the shell to the inner surface of adsorbent also depends on the texture of BPA as reported by a previous literature (Toledo et al., 2005). The dimensions of BPA molecules are accessible to the carbon micropores. As shown in Fig. 4c–d, all adsorbents presented micropores (from 0 to 20 nm), demonstrating that all synthesized

Table 6
Thermodynamic study.

Samples	C_0 (mg/ L)	ΔH (KJ mol^{-1})	ΔS (J mol^{-1} K^{-1})	ΔG (KJ mol^{-1})		
				298 K	318 K	338 K
CSAC	30	13.64	39.7	1.8	1.2	0.14
	40	16.24	46.5	2.3	1.8	0.51
	50	19.33	55.0	2.7	2.3	0.38
	80	19.87	56.0	3.0	2.4	0.74
	100	20.71	57.8	3.3	2.7	0.97
Core-AC	30	32.7	194.6	−25.3	−29.1	−33.1
	40	21.0	117.3	−13.9	−16.55	−18.6
	50	18.3	93.2	−94.6	−11.4	−13.2
	80	31.9	124.9	−54.3	−77.4	−10.4
	100	24.6	97	−43.5	−59.8	−82.6
PAC	30	−36.0	−76.7	−13.5	−10.8	−10.5
	40	−30.0	−58.9	−12.8	−11	−10.6
	50	−13.0	−16.0	−8.6	−8.2	−8.0
	80	−22.8	−58.8	−5.2	−4.3	−2.8
	100	−11.0	−22.9	−4.3	3.9	3.4

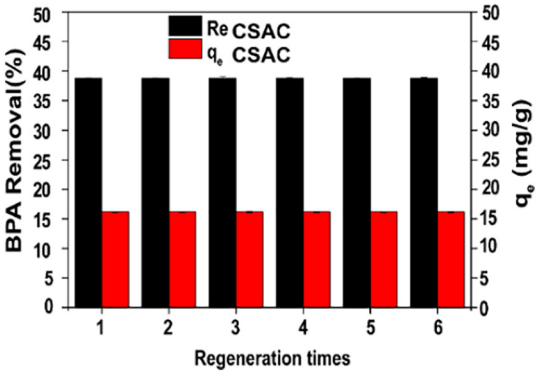

Fig. 9. Thermal regeneration of CSAC.

adsorbents could adsorb more BPA from the water stream. Secondly, BPA molecules reached the external surface of the carbon core and subsequently diffused by the boundary layer to the inner pores of the AC core. The removal of BPA by AC core was confirmed by FTIR (Fig. 11). The new peaks of 3346, 1598, 1509.75, 1219, 828 and 552 cm^{-1}, corresponding to the stretching vibration of —OH, C═C, C—O—C, C═C, C—O, and C—H bonds, indicate BPA was adsorbed on AC core. These FTIR results were in line with the previous reports (Nguyen-Huy et al., 2014; Ullah et al., 2016; Wang et al., 2018; Zhou et al., 2014). Furthermore, the pH of the solution and the pH at the point of zero charges (pH_{pzc}) of the adsorbents constitute other crucial parameters to determine the adsorption mechanisms of organic contaminants. In general, when pH < pH_{pzc}, the AC is cationic, while the acid drugs are neutral (pH < pKa); thus, adsorption possibly requires hydrogen bonding and/or Van der Waals interactions (Baccar et al., 2012). When the pH solution falls into the same value with pH_{pzc}, the surface of the carbon was near to neutral, hence the adsorption mechanism was favored by the increasing of the π -π dispersion interaction (Baccar et al., 2012; Domínguez et al., 2011). In our previous study, the pH_{PZC} value of CSAC was 1.88 (Ndagijimana et al., 2019). In this study at lower pH value, the CSAC was negatively charged while the BPA was in neutral form, indicating that the adsorption possibly required Van der Waals interactions. At pH range between 2 and 7, most of BPA did not dissociate and existed in molecular form, thus the adsorption was dominated by the van der Waals interaction, hydrophobic properties, and π -π dispersion interaction. At high pH value, the adsorbents are in anionic form and BPA is deprotonated to an anion form (BPA^-). Thus, the repulsive electrostatic interactions between the anionic carbon surface and BPA^- would occur and result in the reduction of adsorption capacity. The hydrophobic interaction is also an important property which can determine the adsorption mechanism of BPA on a solid surface (Choi et al., 2005; Sun et al., 2017; Zhou et al., 2014). The hydrophobic interaction was studied according to the value of octanol-water partition coefficient (log $Ko_{w)}$ (Wu et al., 2019). The adsorption efficiency of bisphenols at equilibrium increased accordingly with the raised value of octanol-water partition coefficient (log $K_{ow)}$ (Wu et al., 2019). The log K_{ow} value is a measure of hydrophobicity, therefore, the higher value for BPA (3.1) indicates the higher hydrophobic property which enhances the adsorption of BPA on AC (López-Ramón et al., 2019; Tsai et al., 2006). In short, the possible mechanisms by which CSAC adsorbed

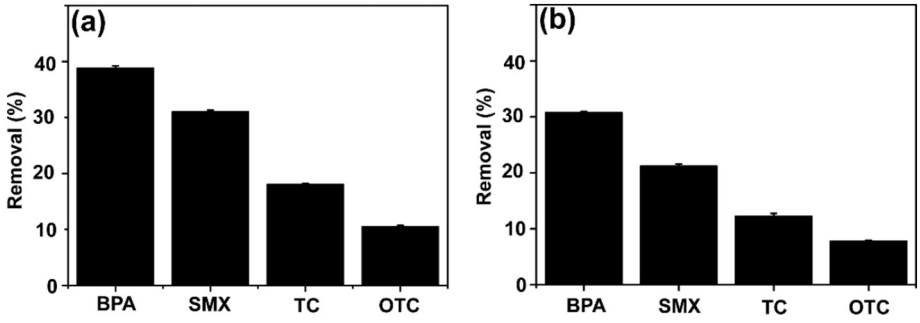

Fig. 10. (a) Adsorption of BPA compare with different antibiotics, (b) the effect of competition.

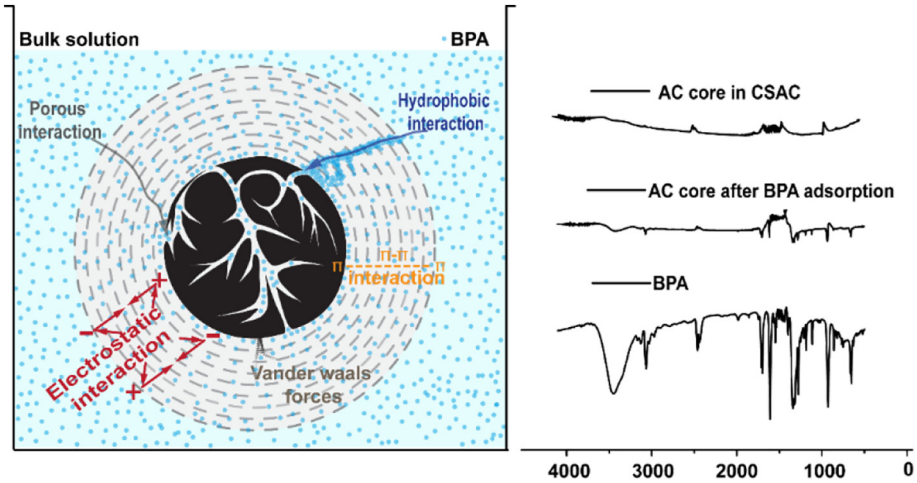

Fig. 11. Schematic of adsorption mechanism.

BPA were related to the pore texture, Vander Waals interaction, π-π dispersion interaction, hydrophobic interaction and electrostatic interaction.

4. Conclusions

The newly CSAC with a small thickness (0.083 cm), high mechanical strength (2.41 MPa), small size (0.82 cm) and lightweight (0.24 g) was synthesized at 1250 °C. The ceramic shell synthesized from the mixture of kaolinite (400 meshes) and coal fly ash (100 mesh) exhibited great protection of activated carbon. The CSAC displayed a beneficial performance on the BPA removal from aqueous solutions. The performance of the material kinetically fitted better to pseudo-second-order and the intraparticle diffusion. In addition, The Freundlich isotherm matched well with the adsorption isotherm. The CSAC exhibited beneficial separation, recyclability and good performance for long-term usability. The potential mechanisms of BPA adsorbed by CSAC rely on the pore texture, Vander Waals interaction, π-π dispersion interaction, hydrophobic and electrostatic interaction. Although the material could be applied in the remediation of aquatic BPA and other endocrine disrupting chemicals (EDCs), further studies investigating such applications in real-world engineered systems are of great necessity.

Acknowledgments

The authors appreciatively acknowledge the financial support from the Strategic Priority Research Program of the Chinese Academy of Sciences [Grant No. XDA23030301], China-Japan Research Cooperative Program [Grant No. 2016YFE0118000], the The Natural Science Foundation of Fujian Province [Grant No. 2019J01135]. The first author also acknowledges the CAS-TWAS President's Fellowship Program for supporting international students in China.

Appendix A. Supplementary data

Supplementary data to this article can be found online at https://doi.org/10.1016/j.scitotenv.2019.06.235.

References

Arampatzidou, A.C., Deliyanni, E.A., 2016. Comparison of activation media and pyrolysis temperature for activated carbons development by pyrolysis of potato peels for effective adsorption of endocrine disruptor bisphenol-A. J. Colloid Interface Sci. 466, 101–112. https://doi.org/10.1016/j.jcis.2015.12.003.

Arnold, S.M., Clark, K.E., Staples, C.A., Klecka, G.M., Dimond, S.S., Caspers, N., Hentges, S.G., 2013. Relevance of drinking water as a source of human exposure to bisphenol A. J. Expo. Sci. Environ. Epidemiol. 23, 137–144. https://doi.org/10.1038/jes.2012.66.

Baccar, R., Sarrà, M., Bouzid, J., Feki, M., Blánquez, P., 2012. Removal of pharmaceutical compounds by activated carbon prepared from agricultural by-product. Chem. Eng. J. 211, 310–317. https://doi.org/10.1016/j.cej.2012.09.099.

Berhane, T.M., Levy, J., Krekeler, M.P.S., Danielson, N.D., 2016. Adsorption of bisphenol A and ciprofloxacin by palygorskite-montmorillonite: effect of granule size, solution chemistry and temperature. Appl. Clay Sci. 132, 518–527. https://doi.org/10.1016/j.clay.2016.07.023.

Bicer, A., 2018. Effect of fly ash particle size on thermal and mechanical properties of fly ash-cement composites. Therm. Sci. Eng. Prog. 8, 78–82. https://doi.org/10.1016/j.tsep.2018.07.014.

Brugnera, M.F., Rajeshwar, K., Cardoso, J.C., Zanoni, M.V.B., 2010. Bisphenol A removal from wastewater using self-organized TIO2 nanotubular array electrodes. Chemosphere 78, 569–575. https://doi.org/10.1016/j.chemosphere.2009.10.058.

Careghini, A., Mastorgio, A.F., Saponaro, S., Sezenna, E., 2015. Bisphenol A, nonylphenols, benzophenones, and benzotriazoles in soils, groundwater, surface water, sediments, and food: a review. Environ. Sci. Pollut. Res. 22, 5711–5741. https://doi.org/10.1007/s11356-014-3974-5.

Çeçen, F., Aktas, Ö., 2011. Activated Carbon for Water and Wastewater Treatment: Integration of Adsorption and Biological Treatment. Wiley-VCH, Weinheim, Germany.

Chen, P.J., Linden, K.G., Hinton, D.E., Kashiwada, S., Rosenfeldt, E.J., Kullman, S.W., 2006. Biological assessment of bisphenol A degradation in water following direct photolysis and UV advanced oxidation. Chemosphere 65, 1094–1102. https://doi.org/10.1016/j.chemosphere.2006.04.048.

Chen, H.W., Liang, C.H., Wu, Z.M., Chang, E.E., Lin, T.F., Chiang, P.C., Wang, G.S., 2013. Occurrence and assessment of treatment efficiency of nonylphenol, octylphenol and bisphenol-A in drinking water in Taiwan. Sci. Total Environ. 449, 20–28. https://doi.org/10.1016/j.scitotenv.2013.01.038.

Choi, K.J., Kim, S.G., Kim, C.W., Kim, S.H., 2005. Effects of activated carbon types and service life on removal of endocrine disrupting chemicals: amitrol, nonylphenol, and bisphenol-A. Chemosphere 58, 1535–1545. https://doi.org/10.1016/j.chemosphere.2004.11.080.

Chowdhury, S., Chakraborty, S., Saha, P., 2011. Biosorption of basic green 4 from aqueous solution by ananas comosus (pineapple) leaf powder. Colloids Surf. B:Biointerfaces 84, 520–527. https://doi.org/10.1016/j.colsurfb.2011.02.009.

Corrales, J., Kristofco, L.A., Steele, W.B., Yates, B.S., Breed, C.S., Williams, E.S., Brooks, B.W., 2015. Global assessment of bisphenol A in the environment: review and analysis of its occurrence and bioaccumulation. Dose-Response 13, 1–29. https://doi.org/10.1177/1559325815598308.

Delgado, L.F., Charles, P., Glucina, K., Morlay, C., 2012. The removal of endocrine disrupting compounds, pharmaceutically activated compounds and cyanobacterial toxins during drinking water preparation using activated carbon—a review. Sci. Total Environ. 435–436, 509–525. https://doi.org/10.1016/j.scitotenv.2012.07.046.

Dogan, M., Abak, H., Alkan, M., 2009. Adsorption of methylene blue onto hazelnut shell: kinetics, mechanism and activation parameters. J. Hazard. Mater. 164, 172–181. https://doi.org/10.1016/j.jhazmat.2008.07.155.

Domínguez, J.R., González, T., Palo, P., Cuerda-Correa, E.M., 2011. Removal of common pharmaceuticals present in surface waters by Amberlite XAD-7 acrylic-ester-resin: influence of pH and presence of other drugs. Desalination 269, 231–238. https://doi.org/10.1016/j.desal.2010.10.065.

Fan, L., Luo, C., Sun, M., Li, X., Qiu, H., 2013. Highly selective adsorption of lead ions by water-dispersible magnetic chitosan/graphene oxide composites. Colloids Surf. B: Biointerfaces 103, 523–529. https://doi.org/10.1016/j.colsurfb.2012.11.006.

Ghaedi, M., Karimi, F., Barazesh, B., Sahraei, R., Daneshfar, A., 2013. Removal of reactive Orange 12 from aqueous solutions by adsorption on tin sulfide nanoparticle loaded on activated carbon. J. Ind. Eng. Chem. 19, 756–763. https://doi.org/10.1016/j.jiec.2012.10.010.

Gong, Z., Li, S., Ma, J., Zhang, X., 2016. Synthesis of recyclable powdered activated carbon with temperature responsive polymer for bisphenol A removal. Sep. Purif. Technol. 157, 131–140. https://doi.org/10.1016/j.seppur.2015.11.040.

Heo, J., Flora, J.R.V., Her, N., Park, Y.G., Cho, J., Son, A., Yoon, Y., 2012. Removal of bisphenol A and 17 beta-estradiol in single walled carbon nanotubes-ultrafiltration (SWNTs-UF) membrane systems. Sep. Purif. Technol. 90, 39–52. https://doi.org/10.1016/j.seppur.2012.02.007.

Hugo, E.R., Brandebourg, T.D., Woo, J.G., Loftus, J., Alexander, J.W., Ben-Jonathan, N., 2008. Bisphenol A at environmentally relevant doses inhibits adiponectin release from human adipose tissue explants and adipocytes. Environ. Health Perspect. 116, 1642–1647. https://doi.org/10.1289/ehp.11537.

Inoue, M., Masuda, Y., Okada, F., Sakurai, A., Takahashi, I., Sakakibara, M., 2008. Degradation of bisphenol A using sonochernical reactions. Water Res. 42, 1379–1386. https://doi.org/10.1016/j.watres.2007.10.006.

Javed, H., Luong, D.X., Lee, C.G., Zhang, D.N., Tour, J.M., Alvarez, P.J.J., 2018. Efficient removal of bisphenol-A by ultra-high surface area porous activated carbon derived from asphalt. Carbon 140, 441–448. https://doi.org/10.1016/j.carbon.2018.08.038.

Jin, H.B., Zhu, L.Y., 2016. Occurrence and partitioning of bisphenol analogues in water and sediment from liaohe river basin and taihu lake, China. Water Res. 103, 343–351. https://doi.org/10.1016/j.watres.2016.07.059.

Kang, J.H., Kondo, F., Katayama, Y., 2006. Human exposure to bisphenol A. Toxicology 226, 79–89. https://doi.org/10.1016/j.tox.2006.06.009.

Kavitha, D., Namasivayam, C., 2007. Experimental and kinetic studies on methylene blue adsorption by coir pith carbon. Bioresour. Technol. 98, 14–21. https://doi.org/10.1016/j.biortech.2005.12.008.

Lagana, A., Bacaloni, A., De Leva, I., Faberi, A., Fago, G., Marino, A., 2004. Analytical methodologies for determining the occurrence of endocrine disrupting chemicals in sewage treatment plants and natural waters. Anal. Chim. Acta 501, 79–88. https://doi.org/10.1016/j.aca.2003.09.020.

Li, Z., Xiang, X., Li, M., Ma, Y.P., Wang, J.H., Liu, X., 2015. Occurrence and risk assessment of pharmaceuticals and personal care products and endocrine disrupting chemicals in reclaimed water and receiving groundwater in China. Ecotox. Environ. Safe. 119, 74–80. https://doi.org/10.1016/j.ecoenv.2015.04.031.

Liu, Z.H., Kanjo, Y., Mizutani, S., 2009. Removal mechanisms for endocrine disrupting compounds (EDCs) in wastewater treatment - physical means, biodegradation, and chemical advanced oxidation: a review. Sci. Total Environ. 407, 731–748. https://doi.org/10.1016/j.scitotenv.2008.08.039.

López-Ramón, M.V., Ocampo-Pérez, R., Bautista-Toledo, M.I., Rivera-Utrilla, J., Moreno-Castilla, C., Sánchez-Polo, M., 2019. Removal of bisphenols A and S by adsorption on activated carbon clothes enhanced by the presence of bacteria. Sci. Total Environ. 669, 767–776. https://doi.org/10.1016/j.scitotenv.2019.03.125.

Marques, S.C.R., Marcuzzo, J.M., Baldan, M.R., Mestre, A.S., Carvalho, A.P., 2017. Pharmaceuticals removal by activated carbons: role of morphology on cyclic thermal regeneration. Chem. Eng. J. 321, 233–244. https://doi.org/10.1016/j.cej.2017.03.101.

Mittal, A., Mittal, J., Malviya, A., Gupta, V.K., 2010. Removal and recovery of chrysoidine Y from aqueous solutions by waste materials. J. Colloid Interface Sci. 344, 497–507. https://doi.org/10.1016/j.jcis.2010.01.007.

Nakanishi, A., Tamai, M., Kawasaki, N., Nakamura, T., Tanada, S., 2002. Adsorption characteristics of bisphenol A onto carbonaceous materials produced from wood chips as organic waste. J. Colloid Interface Sci. 252, 393–396. https://doi.org/10.1006/jcis.2002.8387.

Ndagijimana, P., Xuejiao, L., Guangwei, Y., Yin, W., 2019. Synthesis of a novel core-shell-structure activated carbon material and its application in sulfamethoxazole adsorption. J. Hazard. Mater. 368, 602–612. https://doi.org/10.1016/j.jhazmat.2019.01.093.

Nguyen-Huy, C., Kim, N., Nguyen-Phan, T.-D., Yoo, I.-K., Shin, E.W., 2014. Adsorptive interaction of bisphenol A with mesoporous titanosilicate/reduced graphene oxide

nanocomposite materials: FT-IR and Raman analyses. Nanoscale Res. Lett. 9, 462. https://doi.org/10.1186/1556-276X-9-462.
Ofomaja, A.E., Ho, Y.S., 2007. Equilibrium sorption of anionic dye from aqueous solution by palm kernel fibre as sorbent. Dyes Pigments 74, 60–66. https://doi.org/10.1016/j.dyepig.2006.01.014.
Peng, S., Hao, K.Y., Han, F., Tang, Z., Niu, B.B., Zhang, X., Wang, Z., Hong, S., 2015. Enhanced removal of bisphenol-AF onto chitosan-modified zeolite by sodium cholate in aqueous solutions. Carbohyd. Polym. 130, 364–371. https://doi.org/10.1016/j.carbpol.2015.05.019.
Putra, E.K., Pranowo, R., Sunarso, J., Indraswati, N., Ismadji, S., 2009. Performance of activated carbon and bentonite for adsorption of amoxicillin from wastewater: mechanisms, isotherms and kinetics. Water Res. 43, 2419–2430. https://doi.org/10.1016/j.watres.2009.02.039.
Salvador, F., Martin-Sanchez, N., Sanchez-Hernandez, R., Sanchez-Montero, M.J., Izquierdo, C., 2015a. Regeneration of carbonaceous adsorbents. Part I: thermal regeneration. Microporous Mesoporous Mater. 202, 259–276. https://doi.org/10.1016/j.micromeso.2014.02.045.
Salvador, F., Martin-Sanchez, N., Sanchez-Hernandez, R., Sanchez-Montero, M.J., Izquierdo, C., 2015b. Regeneration of carbonaceous adsorbents. Part II: chemical, microbiological and vacuum regeneration. Microporous Mesoporous Mater. 202, 277–296. https://doi.org/10.1016/j.micromeso.2014.08.019.
Soares, A., Guieysse, B., Jefferson, B., Cartmell, E., Lester, J.N., 2008. Nonylphenol in the environment: a critical review on occurrence, fate, toxicity and treatment in wastewaters. Environ. Int. 34, 1033–1049. https://doi.org/10.1016/j.envint.2008.01.004.
Staples, C. A., Dorn, P. B., Klecka, G. M., O'Block, S. T., Branson, D. R., Harris, L. R., 2000. Bisphenol A concentrations in receiving waters near US manufacturing and processing facilities. Chemosphere 40: 521–525. doi:https://doi.org/10.1016/S0045-6535(99)00288-X.
Sun, W., Wang, C., Pan, W., Li, S., Chen, B., 2017. Effects of natural minerals on the adsorption of 17β-estradiol and bisphenol A on graphene oxide and reduced graphene oxide. Environ, Sci. Nano. 4, 1377–1388. https://doi.org/10.1039/C7EN00295E.
Tan, I.A.W., Ahmad, A.L., Hameed, B.H., 2008. Adsorption of basic dye on high-surface-area activated carbon prepared from coconut husk: equilibrium, kinetic and thermodynamic studies. J. Hazard. Mater. 154, 337–346. https://doi.org/10.1016/j.jhazmat.2007.10.031.
Toledo, I.B., Ferro-Garcia, M.A., Rivera-Utrilla, J., Moreno-Castilla, C., Fernandez, F.J.V., 2005. Bisphenol A removal from water by activated carbon. Effects of carbon characteristics and solution chemistry. Environ. Sci. Technol. 39, 6246–6250. https://doi.org/10.1021/es0481169.
Tonucci, M.C., Gurgel, L.V.A., de Aquino, S.F., 2015. Activated carbons from agricultural byproducts (pine tree and coconut shell), coal, and carbon nanotubes as adsorbents for removal of sulfamethoxazole from spiked aqueous solutions: kinetic and thermodynamic studies. Ind. Crop. Prod. 74, 111–121. https://doi.org/10.1016/j.indcrop.2015.05.003.
Tsai, W.T., Lai, C.W., Su, T.Y., 2006. Adsorption of bisphenol-A from aqueous solution onto minerals and carbon adsorbents. J. Hazard. Mater. 134, 169–175. https://doi.org/10.1016/j.jhazmat.2005.10.055.
Ullah, R., Ahmad, I., Zheng, Y., 2016. Fourier transform infrared spectroscopy of of (bisphenol a). J. Spectrosc. 2016, 5. https://doi.org/10.1155/2016/2073613.
Wang, F., Lu, X., Peng, W., Deng, Y., Zhang, T., Hu, Y.-B., Li, X.-Y., 2017. Sorption behavior of bisphenol A and triclosan by graphene: comparison with activated carbon. ACS Omega 2. https://doi.org/10.1021/acsomega.7b00616.
Wang, L.C., Ni, X.J., Cao, Y.H., Cao, G.Q., 2018. Adsorption behavior of bisphenol A on CTAB-modified graphite. Appl. Surf. Sci. 428, 165–170. https://doi.org/10.1016/j.apsusc.2017.07.093.
Wirasnita, R., Hadibarata, T., Yusoff, A.R.M., Yusop, Z., 2014. Removal of bisphenol A from aqueous solution by activated carbon derived from oil palm empty fruit bunch. Water, Air, Soil, Polut 225, 1–12. https://doi.org/10.1007/s11270-014-2148-x.
Wu, Z., Kong, L., Hu, H., Tian, S., Xiong, Y., 2015. Adsorption performance of hollow spherical sludge carbon prepared from sewage sludge and polystyrene foam wastes. ACS Sustain. Chem. Eng. 3, 552–558. https://doi.org/10.1021/sc500840b.
Wu, P., Cai, Z., Jin, H., Tang, Y., 2019. Adsorption mechanisms of five bisphenol analogues on PVC microplastics. Sci. Total Environ. 650, 671–678. https://doi.org/10.1016/j.scitotenv.2018.09.049.
Xu, J., Wang, L., Zhu, Y., 2012. Decontamination of bisphenol A from aqueous solution by graphene adsorption. Langmuir 28, 8418–8425. https://doi.org/10.1021/la301476p.
Yuan, Y., Gu, P., Yang, Y., Zhang, G., 2016. Regeneration of PAC used for reverse osmosis concentrate treatment by wet oxidation. J. Ind. Eng. Chem. 34, 98–104. https://doi.org/10.1016/j.jiec.2015.10.043.
Zhou, Y.B., Chen, L., Lu, P., Tang, X.Y., Lu, J., 2011. Removal of bisphenol A from aqueous solution using modified fibric peat as a novel biosorbent. Sep. Purif. Technol. 81, 184–190. https://doi.org/10.1016/j.seppur.2011.07.026.
Zhou, X., Wei, J., Liu, K., Liu, N., Zhou, B., 2014. Adsorption of bisphenol A based on synergy between hydrogen bonding and hydrophobic interaction. Langmuir 30, 13861–13868. https://doi.org/10.1021/la502816m.